

Study of the Formation of a Solid Electrolyte Interphase (SEI) on a Silicon Nanowire Anode in Liquid Disiloxane Electrolyte with Nitrile End Groups for Lithium-Ion Batteries

Yonatan Horowitz,^{*[a]} Ido Ben-Barak,^[a] Dan Schneier,^[a] Meital Goor-Dar,^[a] Johannes Kasnatscheew,^[b] Paul Meister,^[b] Mariano Grünebaum,^[b] Hans-Dieter Wiemhöfer,^[b] Martin Winter,^[b, c] Diana Golodnitsky,^{*[a]} and Emanuel Peled^{*[a]}

The chemical compatibility of the various compounds and elements used in lithium-based batteries dictates their safe operation parameters and performance. The lithium salt Li-bis(trifluoromethanesulfonyl)imide (LiTFSI) has many advantages over the common LiPF₆ salt as it does not react with water impurities to form, for example, hydrofluoric acid. To further accommodate safe-operation chemistry, we use a non-volatile disiloxane-based solvent 1,3-bis(cyanopropyl)tetramethyldisiloxane (TmdSx-CN). This is a liquid disiloxane functionalized with terminal nitrile groups. In this paper, we report on the electrochemical characterization and the composition of the solid electrolyte interphase (SEI) of 1 mol kg⁻¹ LiTFSI dissolved in TmdSx-CN in silicon-lithium batteries. Specifically, we study the

SEI formation on silicon nanowire anodes and its composition by several ex-situ surface techniques (XPS, SEM), and in-situ via polarization modulation infrared reflectance absorption spectroscopy (PM-IRRAS). We evaluate the potential application of TmdSx-CN to silicon-lithium batteries and conclude that the addition of fluoroethylene carbonate (FEC) at low concentrations (10 wt %) is essential to the formation of an effective SEI. We anticipate that our study will encourage the investigation, design and use of siloxane-based solvents as safer alternatives to common solvents used in Li-ion batteries, and specifically as candidate solvents in Li-metal and silicon-anode based batteries.

1. Introduction

The technology of the lithium-ion battery has proven to be one of the most promising energy-storage technologies, with applications ranging from electrical toys to vehicles.^[1–3] As such, its safety is of crucial importance. This requirement frequently hinders consumer-market designs that require either a high energy density (as found in portable devices) or high-power throughput (e.g., electric vehicles) because the chemical

composition of the lithium-ion battery dictates its energy profile.

The most commonly used electrolytes consist of carbonate-containing liquid electrolytes with lithium hexafluorophosphate (LiPF₆) as conducting salt. The main disadvantage of both carbonate-based solvents and LiPF₆ salt is their sensitivity to moisture in addition to insufficient thermal and safety aspects.^[4,5] An alternative to LiPF₆ is lithium perchlorate (LiClO₄). However, while it has a higher thermal stability than LiPF₆, it suffers from low anodic stability (<4.5 V vs. Li/Li⁺).^[6] As opposed to this, sulfonylimide-based lithium salts dissolved in carbonate-type solvents show an anodic stability greater 5 V vs Li/Li⁺. However, the greatest drawback of sulfonylimide-based electrolytes is the anodic dissolution of aluminium current collectors,^[7] which depends on the used solvent.^[8] Other drawbacks of today's electrolytes are: insufficient chemical stability, risk of thermal runaway due to the reaction of the solvents and salts with the anode and the cathode at elevated temperatures, relatively high volatility of linear carbonates and gas formation during the first few charge cycles,^[9–11] and at elevated-temperature storage.^[12] Therefore, there is ongoing research to develop novel battery electrolytes (solvents and conductive salts) that will avoid thermal, chemical and environmental issues, will produce an effective solid electrolyte interphase (SEI) on the anode and remain affordable.^[13,14] Recently, the silicon anode has been studied as an alternative to graphite in the lithium-ion battery because of its better

[a] Dr. Y. Horowitz, I. Ben-Barak, D. Schneier, Dr. M. Goor-Dar, Prof. D. Golodnitsky, Prof. E. Peled
School of Chemistry
Faculty of Exact Sciences and Applied Materials Research Centre
Tel Aviv University
Tel Aviv, 6997801, Israel
E-mail: horowitz2@mail.tau.ac.il
golod@tauex.tau.ac.il
peled@tauex.tau.ac.il

[b] Dr. J. Kasnatscheew, Dr. P. Meister, Dr. M. Grünebaum, Prof. H.-D. Wiemhöfer, Prof. M. Winter
Forschungszentrum Jülich GmbH
Helmholtz-Institute Münster, IEK 12
Corrensstrasse 46, 48149 Münster, Germany

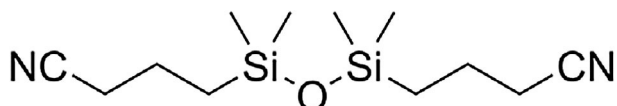
[c] Prof. M. Winter
MEET Battery Research Center
University of Münster
Corrensstrasse 46, 48149 Münster, Germany

 Supporting information for this article is available on the WWW under <https://doi.org/10.1002/batt.201800123>

 An invited contribution to a Special Issue on SEI and Interphases at Electrodes

safety and much higher capacity. However, as a result of large volume changes during charge (lithium uptake) and discharge (lithium release), an ineffective SEI is formed. Under these conditions, the lithiated silicon reduces the electrolyte and shortens the life of the battery. Study and improvement of the SEI on silicon is a crucial issue.

The incorporation of siloxane^[15,16] and silane^[17] based low viscosity solvents as electrolytes in lithium-ion batteries can circumvent some of the abovementioned drawbacks, namely chemical stability, relatively high volatility and temperature endurance, while exhibiting a wide potential window. Here, we report the results obtained from characterizations of SEI formed on silicon nanostructures in disiloxane-based 1,3-bis(cyanopropyl)tetramethyldisiloxane, a disiloxane with nitrile end groups (TmdSx-CN, refer to Scheme 1) and compare it to an SEI formed



Scheme 1. Novel disiloxane solvent, 1,3-bis(cyanopropyl)tetramethyldisiloxane (TmdSx-CN).

with a fluorocarbon additive ubiquitous to silicon anode based batteries.^[18] We emphasize the critical role of fluoroethylene carbonate (FEC) addition in producing an effective SEI enabling cycling stability and faster C-rate.

Several characterisation techniques were used: electrochemical impedance spectroscopy (EIS), scanning electron microscopy (SEM), X-ray photoelectron spectroscopy (XPS) and in-situ polarization-modulation infrared-reflectance absorption spectroscopy (PM-IRRAS).

Our paper is divided into two main parts. In the first part, we present results obtained with in-situ techniques (EIS, PM-IRRAS) and in the second part we show data acquired by ex-situ methods (SEM, XPS).

2. Results and Discussion

We have tested the electrochemical properties of disiloxane (TmdSx-CN, refer to Scheme 1) in various half-cell configurations, and at two compositions: with and without fluoroethylene carbonate (FEC).

In order to obtain the best solid electrolyte interphase (SEI) of this novel disiloxane electrolyte, we have chosen to cycle our half-cells at low currents (galvanostatically).^[19] In symmetrical Li cells, (i.e., Li vs Li, Figure S1), constant-current/constant-voltage (CC/CV) prolonged galvanostatic cycling was carried out and their stability vs metallic lithium was established. The stability of the electrolyte during lithium deposition/dissolution on stainless-steel electrodes (Figure S2) was studied. Figure 1 presents the overall performance of two types of Li/Si coin cells (with and without FEC) cycled (from open-circuit voltage (~2.7 V) at 100 μ A between 0.05 V and 1.0 V. All the following cells were in a Li vs silicon nanowires (SiNWs) half-cell configuration (with

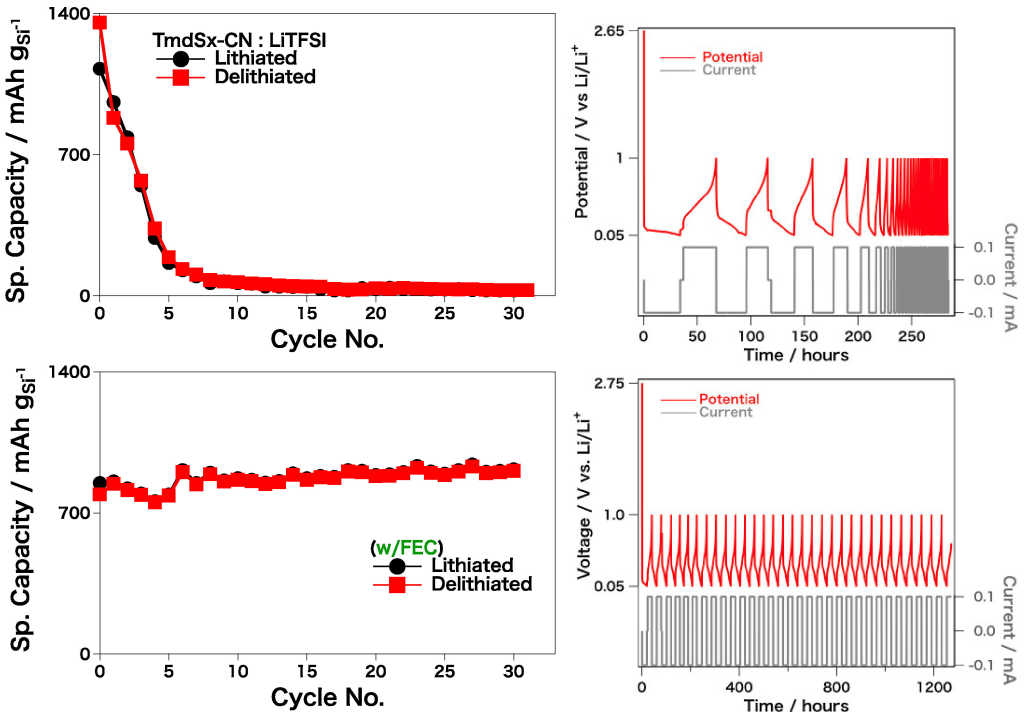


Figure 1. Plots of silicon specific capacity vs cycle number for two electrolyte compositions and their related charging/discharging curves. a) 1 mol kg⁻¹ LiTFSI in TmdSx-CN, SiNWs loading of 2 mg_{Si} cm⁻². b) 1 mol kg⁻¹ LiTFSI in TmdSx-CN with 10%(wt) FEC and a SiNWs loading of 0.71 mg_{Si} cm⁻². All coin cells were in a two-electrode configuration and were cycled from open-circuit voltage (~2.7 V) at 100 μ A to 0.05 V, and then between 0.05 V and 1.0 V. Their related charging/discharging curves are presented in c) for the TmdSx-CN, and d) for TmdSx-CN with 10% wt FEC.

equivalent Si loading of $2 \text{ mg}_{\text{Si}} \text{ cm}^{-2}$). It is clear that without FEC, the silicon capacity is dramatically reduced within the first five cycles (Figure 1a).

It is suggested that this poor cyclability originates from the inability of disiloxane to produce a good SEI, since cycling the neat (no salt) TmdSx-CN in a SiNWs vs Li half-cell resulted in a reduction current which increased with increasing cycle number (Figure S3). When the capacity is calculated, we note that it fell from $\sim 1400 \text{ mAh g}_{\text{Si}}^{-1}$ to $\sim 100 \text{ mAh g}_{\text{Si}}^{-1}$ after only five cycles. This quick cell death is explained by a model in which the secondary porous siloxane-based SEI is quickly clogged by the insoluble reduction products, which do not conduct Li^+ . This explanation is based on the proposed two-stage SEI-formation model;^[19] at first, during the initial lithiation, a compact SEI forms on the surface of the silicon nanowires while the SiNWs expand in volume. With the first charge, the SiNWs shrink in size and, accordingly, their surface area decreases. This surface decrease squeezes out any extra SEI materials caged in the primary compact SEI, and these in turn, form a secondary porous layer whose pores are filled with electrolyte. With cycling, the thickness of the secondary porous layer grows, and its porosity decreases, subsequently limiting the transport of lithium ions and inevitably causing a loss of capacity and power.

In order to further understand the changes that occur in the SiNW anodes during cycling, we carried out electrochemical-impedance-spectroscopy (EIS) tests. The selected Nyquist plots are presented in Figure 2.

The five-component equivalent circuit used for the analysis of the EIS spectra (inset in Figure 2a) includes the following components: R_1 (R_{bulk}) – the resistance of the electrolyte, R_2 ($R_{\text{SEI},\text{Si}}$) – the resistance of the SEI, C_2 – the capacitance of the SEI layer ($C_{\text{SEI},\text{Si}}$), R_3 , and C_3 are the resistance ($R_{\text{SEI},\text{Li}}$), and the capacitance ($C_{\text{SEI},\text{Li}}$) of the SEI layer on the metallic lithium. The components values are summarized in Table 1. In Figure 2a, the increased values of the Nyquist-plot intersections in the high-frequency region will be noted. These are translated to increased bulk-resistance (R_{bulk}) values. Therefore, it seems that a substantial portion of the electrolyte reduction products, do not form a compact SEI but diffuse into the bulk of the electrolyte and precipitate into the separator. Also, in Figure 2a we see that the $C_{\text{SEI},\text{Si}}$ of the neat siloxane-based electrolyte maintains similar values of $\sim 2.30 \mu\text{F}$ and $1.50 \mu\text{F}$, corresponding to the first and tenth lithiations. Qualitatively, the thickness of the SEI is proportional to the reciprocal of the SEI capacitance value.^[19] This corresponds to the two-stage SEI failure mechanism, previously explained, in which the thickness of the SEI grows with cycle number, leading to a reduced capacity. By contrast, $C_{\text{SEI},\text{Si}}$ of the electrolyte containing FEC, presented in

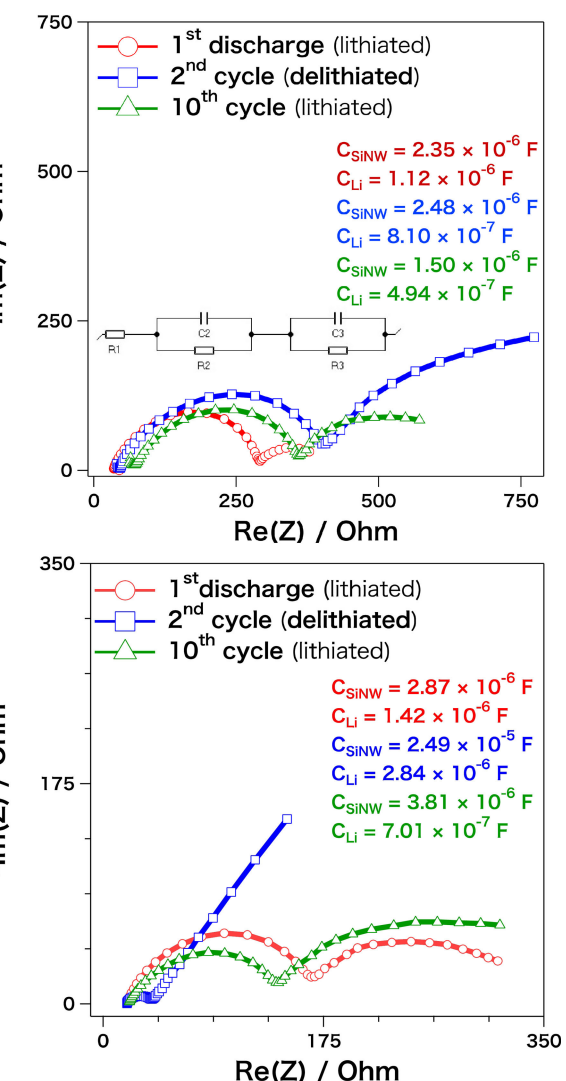


Figure 2. EIS spectra after the first, second and tenth cycles of a) top 1 mol kg^{-1} LiTFSI:TmdSx-CN b0, bottom 1 mol kg^{-1} LiTFSI:TmdSx-CN with 10% (wt) FEC.

Figure 2b, increases slightly from $\sim 2.9 \mu\text{F}$ after the first lithiation, to $\sim 3.8 \mu\text{F}$ after the tenth. Also, $R_{\text{SEI},\text{Si}}$, represented by the diameter of the second semicircle, is much smaller with FEC after the second delithiation, indicating a thinner SEI having a higher content of polymer formed on the reduction of FEC.^[20-22]

The equivalent circuit suggested here, also has components associated with the SEI formed on the lithium metal. The capacitance of the SEI produced from the reduction of electrolyte, $C_{\text{SEI},\text{Li}}$, falls from $\sim 2.5 \mu\text{F}$ to $\sim 0.5 \mu\text{F}$ within ten cycles. Together with the increase in the total resistance of both SEIs,

Table 1. The five-component equivalent circuit values used for the analysis of the EIS spectra.

TmdSx-CN					TmdSx-CN w/FEC (10% wt)					
	R_{bulk} [Ω]	$R_{\text{SEI},\text{Si}}$ [Ω]	$C_{\text{SEI},\text{Si}}$ [μF]	$R_{\text{SEI},\text{Li}}$ [Ω]		R_{bulk} [Ω]	$R_{\text{SEI},\text{Si}}$ [Ω]	$C_{\text{SEI},\text{Si}}$ [μF]	$R_{\text{SEI},\text{Li}}$ [Ω]	$C_{\text{SEI},\text{Li}}$ [μF]
1 st discharge	36.25	201.9	2.35	42.34	1.12	20.71	112.2	2.87	27.04	1.42
2 nd cycle	48.58	265.9	2.48	72.59	8.10	19.35	10.77	2.49	8.715	2.84
10 th cycle	94.97	258.6	1.50	72.34	0.494	25.9	42.66	3.81	18.67	7.01

$R_{SEI,Li}$ and $R_{SEI,SiNW}$ from $\sim 244 \Omega$ to $\sim 330 \Omega$, this leads to the assumption that the disiloxane reduction results in a porous SEI layer that has a relatively high resistance. The addition of FEC also has a beneficial effect on the SEI formed on the lithium electrode. Not only are the $C_{SEI,Li}$ values higher than those of the equivalent neat electrolyte, but the initial total resistance ($\sim 160 \Omega$) is lower than that of the pristine (free-of-FEC) disiloxane electrolyte ($\sim 280 \Omega$). Moreover, the total resistance decreases with cycling to $\sim 87 \Omega$. This behaviour shows the necessity of mixing FEC with the disiloxane electrolyte. We notice that in the EIS high-frequency range a deformed semicircle is present so we simulated it by superimposing two semicircles, i.e., two RC combinations and a bulk resistance component. While the EIS high-frequency range with its capacitance and resistance is explained by our five-component equivalent circuit, we cannot say the same for the low-frequency range typically dominated by the solid-state diffusion of lithium ions alloying with the bulk of the SiNW. When such diffusion takes place in SiNWs, one expects to see a clear impedance element due to a semi-infinite diffusion into the SiNWs which would give rise to a linear slope in the Nyquist plot even at moderate frequencies. For very small frequencies, the appearance should change further, as the concentration gradients oscillate over the entire width of the nanowires or are blocked at the metallic current collector interface.^[23] Except for the delithiation of the FEC:TmdSx-CN mixture (Figure 2.b), this is not the case. We therefore assume that the secondary SEI formed has a porous nature which leads to smaller diffusion constants through the secondary layers.^[24]

In Figure 3a we present the vibrational spectrum and the relevant vibration assignments of the neat TmdSx-CN solvent, and of the electrolyte solution (1 mol kg⁻¹ LiTFSI in TmdSx-CN) recorded by attenuated total reflection–Fourier transform infrared spectroscopy (ATR-FTIR).^[25–32] To test the chemical stability of both solutions to oxygen and moisture we exposed both (neat disiloxane, and electrolyte) to the atmosphere for 10 minutes.

On the basis of our ATR-FTIR spectra, we concluded that the disiloxane is not too hygroscopic. However, the electrolyte absorbs water because of the hygroscopic LiTFSI, which is evident by the presence of two characteristic broad residual-water peaks at 1630 cm⁻¹ and 3500 cm⁻¹ (refer to Supporting Information, Figure S3).^[33–35]

To characterize the composition of the SEI on the silicon nanostructure anodes under cycling conditions, we applied polarization-modulation infrared-reflectance absorption spectroscopy (PM-IRRAS). We scanned two electrolyte compositions – with and without 10% (wt) FEC – at open-circuit voltage (OCV), and after cycling. The Si–O (siloxane bond) and R–C=O (carbonate groups) are detected in the spectra in the range of 800 cm⁻¹ to 2400 cm⁻¹ (Figure 3b). Figure 3c is focused on the C–H stretching range found between 2780 cm⁻¹ and 3400 cm⁻¹. To view changes in the formation of the SEI we have subtracted and normalized the spectra as is done in studies of subtractively normalized interfacial Fourier-transform infrared-reflection spectroscopy (SNIFTIRS).^[36]

$\Delta R/R = (R_{OCV} - R_{cycled})/R_{OCV}$ where R_{OCV} stands for the spectrum obtained at OCV, and R_{cycled} represents the spectrum obtained after cycling at $\pm 100 \mu\text{A}$ between 1.0 V and 0.05 V for ten cycles. Accordingly, the vibrations of the products (i.e. the SEI materials) will have a “negative” peak. We deduce from the profile of the cycled TmdSx-CN:LiTFSI that the SEI consists mainly of dissociated nitrile groups such as amine, amide. We propose that the nitrile groups are substituted by carbonyl groups since new vibrations associated with esters appear at 1773 cm⁻¹,^[26,37,38] although, the C=O vibration at 1773 cm⁻¹ might be due to soluble imide anion (TFSI⁻) present in the disiloxane solvent.^[39] After examining the C–H range (Figure 3c), we further suggest the presence of silicon–carbon^[40] species on the oxidised silicon surface ($O_xSi-O-CH_3$) as the typical asymmetric stretch of the methyl group is present at 2990 cm⁻¹.^[41] The presence of a moderate peak at 1598 cm⁻¹ that corresponds to cyano–vinyl bonds, brings us to infer that the disiloxane bond (Si–O–Si) can break under silicon lithiation potentials.

The spectrum above 3100 cm⁻¹ is broad and may consist of Si–OH vibrations and asymmetric CH₂ stretch typical of vinyl groups.^[26] Naturally, the mere appearance of new peaks after cycling supports our suggestions that an SEI is formed. To validate our claim that the nitrile end groups undergo reduction and detachment we conducted XPS measurements on the SiNW anode after cycling in neat TmdSx-CN in a Li vs SiNWs half-cells. The XPS data and analysis based on previous work^[42,43] are presented in Figure 4 while the CV results are displayed in Figure S3.

Cycling the disiloxane:LiTFSI electrolyte with 10% (wt) FEC yields an intense peak at 1295 cm⁻¹. We assign this to the formation of Li–alkyl species.^{[38][44]} We did not discern a poly (FEC) peak expected at 1805 cm⁻¹.^[40,45] This might be explained by either a low signal-to-noise ratio as a relative high concentration of FEC (above 15 wt%) is needed to produce a prominent peak, or that the peak is enveloped by the broader and more intense asymmetric peak at about 1830 cm⁻¹.^[46] We assign the peak at 1830 cm⁻¹ to the carbonyl group of the FEC, as well as to R–CF=O reduction products reported in the presence of lithium.^[47] The addition of 10 wt% FEC enables the presence of TmdSx-CN solvent near the SiNWs surface. We base this assumption on the appearance of peaks between 2200 cm⁻¹ and 2400 cm⁻¹ attributed to alkyl nitriles.^[26] Here, we can assign another peak at about 2360 cm⁻¹ corresponding to the interaction of nitrile groups with oxygen atoms. The $-C\equiv N\rightarrow O$ effect is supported by presence of another peak at 1378 cm⁻¹ related to the N–O stretching vibration. We propose that these vibrations may originate from FEC molecules and disiloxane molecules co-adsorption (or presence) in the SEI pores. Lastly, we attribute the strong peak at 2470 cm⁻¹ to the coordination of nitriles by lithium ions ($-C\equiv N\rightarrow Li^+$), resulting in higher intensity and blue shift of the nitrile $-C\equiv N$ vibration. Additional peaks in the C–H stretch region at about 2800 cm⁻¹, 3000 cm⁻¹ and 3300 cm⁻¹ indicate that alkyls are formed only in the presence of FEC.

Next, in order to compare the SEI chemical composition and morphology with and without 10% FEC, we carried out ex-

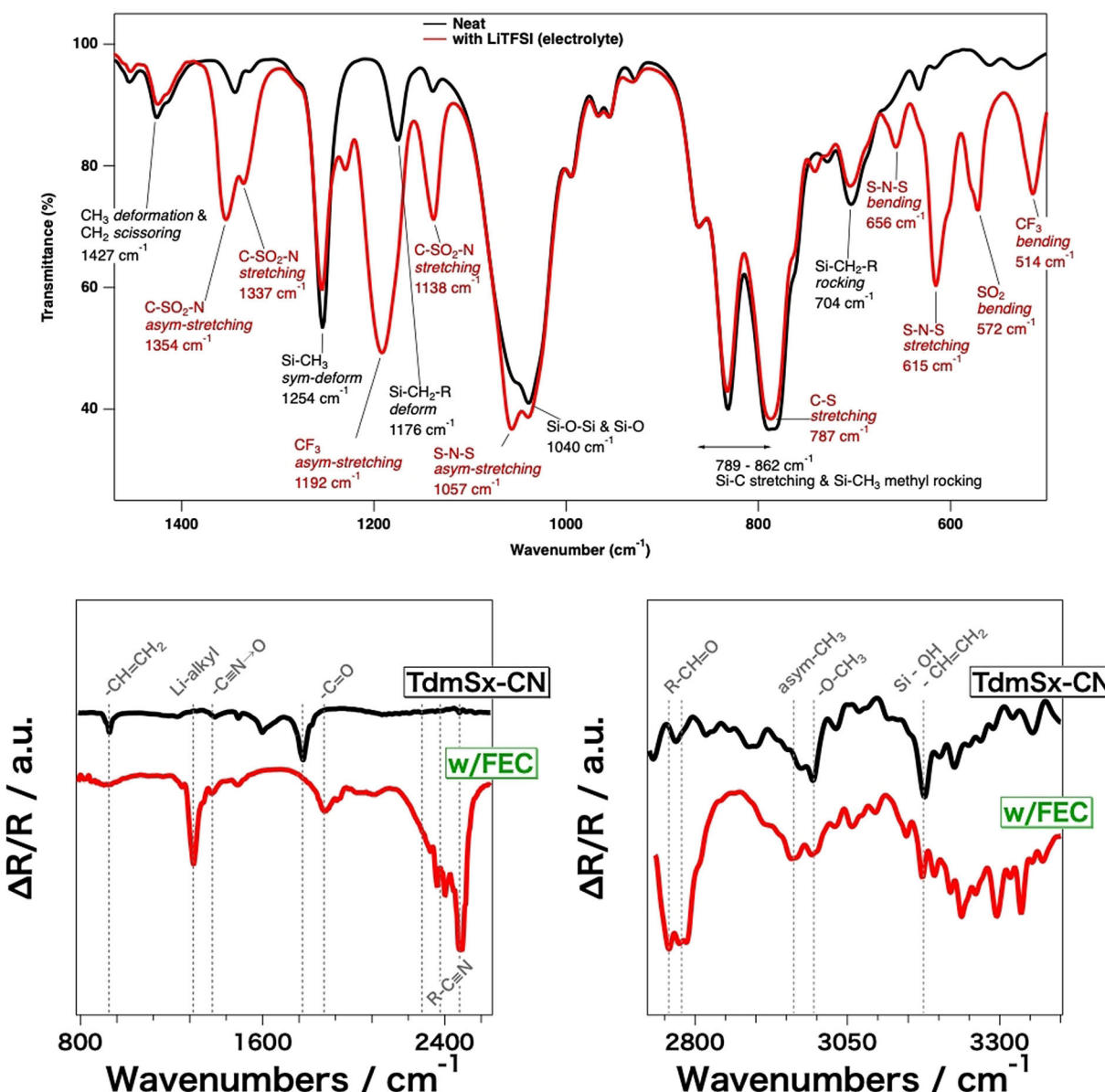


Figure 3. a) The ATR-FTIR spectrum of neat TmdSx-CN (black), and with 1 mol kg⁻¹ LiTFSI (red), spectra with relevant vibration assignments. b) In-situ PM-IRRAS spectra in the range of 800–2400 cm⁻¹ of silicon nanowires under OCV conditions relative to the spectrum after cycling at $\pm 100 \mu\text{A}$ between 1.0 V and 0.05 V for 10 cycles of 1 mol kg⁻¹ LiTFSI: TmdSx-CN, as well as the same electrolyte with the addition of 10% (wt) FEC at OCV, and after cycling. c) In-situ PM-IRRAS spectra of the same samples and conditions now in the 2780–3400 cm⁻¹ range.

situ X-ray photoelectron spectroscopy (XPS) and depth profiling, along with scanning electron microscopy (SEM). In general, the SEI is a mosaic of inorganic and organic reduction products.^[19] The relative amounts of inorganic and organic products as well as their chemical formulas, depend on the electrolyte composition and electrode material.

To better distinguish between the inorganic and organic products we washed the cycled silicon nanowire anodes in either water or dimethyl carbonate (DMC). Washing with water removes some inorganic residues (salts, etc.) while keeping the immiscible organic SEI products. Naturally, washing the cycled anodes with DMC removes some of the organic phase so that the inorganic species are more pronounced. To present our results in a clear and orderly fashion, we have further divided

the ex-situ XPS section into two parts. In the first we present the results from samples washed in DMC. In the second part the same samples are washed in water only.

2.1. X-Ray Photoelectron Spectroscopy

Here, we review the XPS depth-profile spectra of carbon (C 1s), silicon (Si 2p), oxygen (O 1s), fluorine (F 1s), and lithium (Li 1s). By so doing, we can identify the main SEI components and gain knowledge of its structure. The spectra of the above elements, taken at the surface, and after 22 minutes of sputter, together with their peak assignments are presented in Figure S4 and Figure S5. In Figure 5, we present the elemental atomic

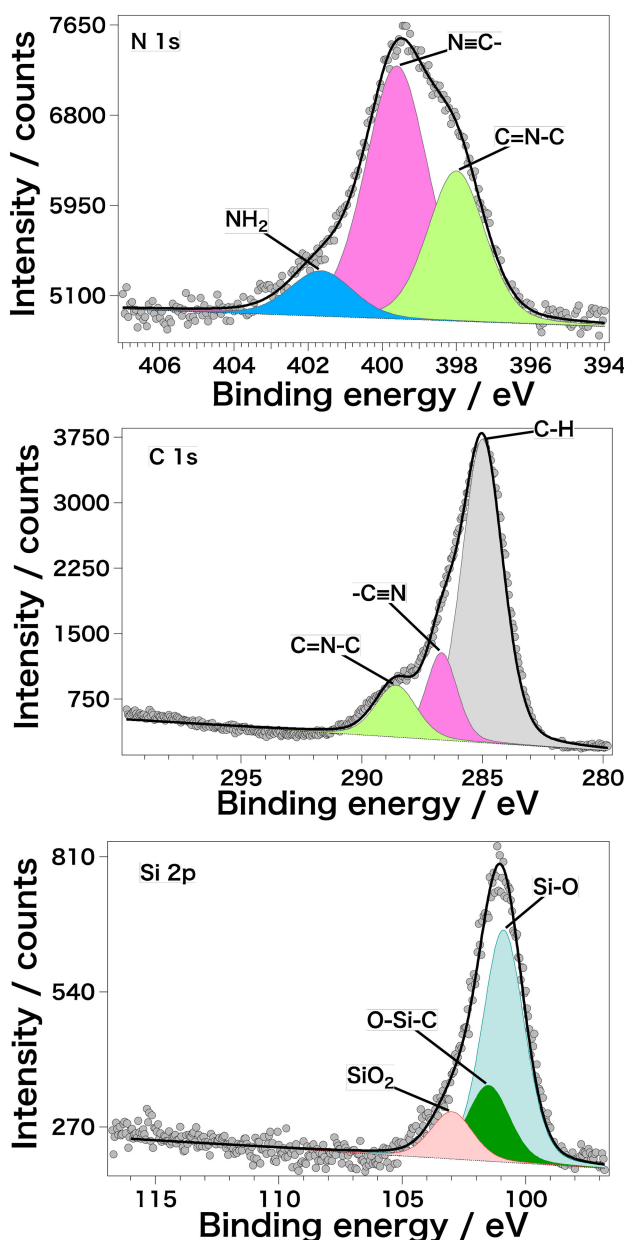


Figure 4. The N 1s, C 1s, and Si 2p XPS spectra, in the surface of SiNWs, after cycling 10 times between 1.0 V and 0.02 V at 1 mV/s, in a Li vs silicon nanowires half-cell containing neat TmdSx-CN (i.e., no salt was added).

concentration as a function of sputter time, electrolyte composition (with or without FEC) and aqueous or non-aqueous wash, after cycling at $\pm 100 \mu\text{A}$ between 1.0 V to 0.05 V for 30 cycles.

2.2. TmdSx-CN: LiTFSI Cycled Anodes, Washed with DMC

On the outer layer of the SEI, the layer facing the electrolyte solution (defined as $t_{\text{sputter}}=0$ minutes), we note the presence of Li_2CO_3 as evident by peaks of C 1s at 290.1 eV, O 1s at 531.65 eV, and Li 1s at 55.1 eV.^[48] We also detect Li_2O with its characteristic peaks of O 1s at 528.6 eV, and Li 1s at 54.45 eV.^[48]

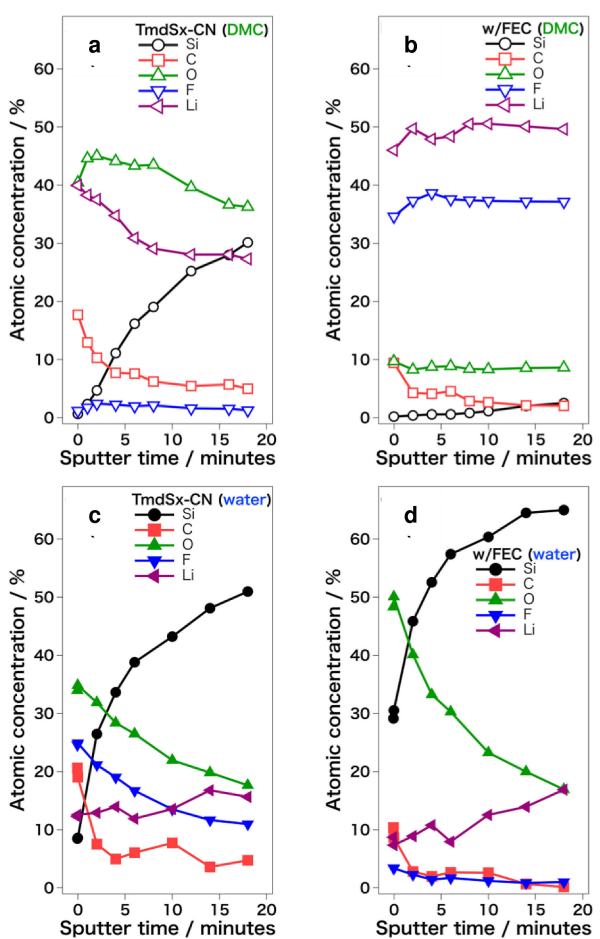


Figure 5. The depth profile of washed anodes. We plot the atomic concentration of Si, C, O, F and Li as functions of sputter time: neat electrolyte, a) DMC wash and c) water wash, and electrolyte with FEC, b) DMC wash and d) water wash.

The Si–O bond has a very broad Si 2p peak at 100.95 eV. Another, at 103 eV has an intensity on the same scale as the signal-to-noise ratio. The C 1s signal at 285.0 eV, typically associated with carbon–carbon and carbon–hydrogen bonds, is very prominent. The signal of silicon increases quickly during sputtering, from zero to 30% after 17 minutes of sputtering. It is a clear indication of the existence of various siloxane moieties (Si–O–R) in the SEI.

After 22 minutes of sputter (refer to Figure S4 and S5) the signals of Si 2p at 101.3 eV and at 101.7 eV, together with the C 1s at 282 eV, all associated with the C–Si–O bond, are still apparent. This supports our suggestion that we indeed detect siloxane-reduction products in the SEI.

2.3. TmdSx-CN: LiTFSI with FEC 10%(wt) Washed with DMC

We suggest that the addition of FEC resulted in mainly fluorinated-rich SEI with LiF^[22,49] and trapped LiTFSI.^[48] This is because the C 1s XPS spectrum is dominated by carbon–fluorine bonds at 291.8 eV (LiTFSI, C–F_x) and at 287.1 eV assigned to C–CF_x. The presence of LiTFSI is evident by the relatively high

atomic concentrations of the Li 1s peak at 57.8 eV and the F 1s peak at 57.8 eV. We suggest that the SEI contains lithium-fluoride (LiF) nanoparticles both on the surface and in the bulk, since a Li 1s peak at 56.6 eV and an F 1s peak at 686.5 eV remain visible throughout the sputtering process. Before sputtering and within the first few sputter cycles the LiF peak is screened by those we associate with Li_2CO_3 and residual LiTFSI (Figure S4). However, after 22 minutes of sputtering, the LiF peak is detectable and larger than that of Li_2CO_3 .

On the basis of our XPS analysis of cycled electrodes washed in DMC, we propose that the addition of FEC produces an SEI comprising LiF nanoparticles in the bulk of the SEI close to the surface of the silicon nanowires. It was suggested that LiF nanoparticles precipitate on the electrode's surface under a certain diameter an ultra-microelectrode-like surface termination may form. In turn, this termination leads to a uniform diffusion field giving rise to more uniform stripping and plating of lithium on copper current collectors.^[46] In addition, we suggest that the presence of fluorine throughout the SEI may indicate that some of the FEC reduction products encapsulate residual lithium anion salt (TFSI). This unique encapsulation property can explain how siloxane-based solvents hinder aluminium pitting as was reported by Pohl et al.^[15,16]

2.4. TmdSx-CN: LiTFSI Washed with Water

Although washed in water, it is clear that the surface of the SiNWs retains residual LiTFSI, since we detect the combined peaks of C 1s at 293.35 eV (C-F₃ group) and Li 1s at 56.1 eV but no F 1s peak at 686.5 eV (i.e., no LiF is present). In the SEI we also detect Si 1s peaks at 103.0 eV and 101.7 eV that are associated with siloxane (Si—O), and organic silicon compounds (e.g., Si—O—C bonds).^[50,51] Thus, we suggest that siloxane-reduction species are incorporated into the SEI. This trend was maintained on continuing sputtering for up to six minutes. After that, the C 1s peak at 293 eV (LiTFSI)^[48] vanished and the stainless-steel mesh, indicated by the Fe 3p peak at ~56 eV, was found. The detection of Fe 3p explains the increase in the Li 1s atomic concentration since the two are close in energy.

2.5. TmdSx-CN:LiTFSI with FEC 10%(wt) Washed with Water

In this case, the water wash resulted in low atomic concentrations of carbon and fluorine but rich in silicon, oxygen, and lithium in the composition of the SEI. As expected, the C 1s spectra are enriched with carbonaceous species, like the compounds containing carbon-carbon bonds (285.0 eV), $(\text{CH}_2\text{OCO}_2\text{Li})_2$ at 286.8 eV, various oligomers, e.g. R-CH₂OLi (288.9 eV) and ROCO₂Li (292.9 eV). The assignments of these carbon peaks coincide with a broad O 1s peak at 532.4 eV and a Li 1s peak at 55.65 eV, thus supporting the presence of ROCO₂Li moieties. In addition, in the Si 2p spectrum we detected Si—O bonds (Si 2p peak at 103 eV) and elemental Si at 99.0 eV. After two minutes of sputtering, the C 1s spectrum is transformed to a single peak at 285.0 eV and the O 1s peak shifts from 532.4 eV

to 533.2 eV. Interestingly, there are also increases in the intensities of the siloxane peak at 103 eV and the organic-silicon peak at 101.7 eV. After 14 minutes of sputtering, the siloxane peak vanishes.

On the basis of our XPS analysis of cycled electrodes washed in water, we propose that the addition of FEC caused the formation of an SEI containing oligomers in addition to siloxane-reduction species. These oligomers were not present in the SiNWs cycled in pristine LiTFSI TmdSx-CN electrolyte.

2.6. Scanning Electron Microscopy

To investigate the SEI morphology, we have obtained images of the surface of fresh SiNW electrodes, soaked in electrolyte and cycled at $\pm 100 \mu\text{A}$ between 1.0 V to 0.05 V for 30 cycles, by SEM (Figure 6). In general, the active material in the anodes consists solely of long, thin silicon nanowires and short, bulky silicon nanoparticles. As with the XPS samples, these were also cut into four pieces and washed in either DMC or water before their transfer to the SEM instrument.

2.7. TmdSx-CN: LiTFSI Cycled

In Figures 6b and 6d, are presented the surface images of SiNWs cycled (10 cycles at $\pm 100 \mu\text{A}$ between 1.0 V and 0.05 V) after being washed in water or DMC. We were able to cycle the SiNWs in TmdSx-CN:LiTFSI for fewer than five full charge-discharge cycles before cell death. When washed in water (Figure 6b), the SiNW surface layer seems ragged, but in the high-magnification micrographs (Figure 6b, inset) the surface appears to be coated. On the other hand, when washed in DMC, (Figure 6d) the SiNW layer appears to be broken into distinguishable islands. Each island has a dense coating layer. We therefore suggest, that although an SEI was formed on the SiNW surface, it consists mainly of inorganic salts.

2.8. TmdSx-CN:LiTFSI with FEC 10%(wt) Cycled

From a comparison of Figure 6b (no FEC) with 6c (with FEC), it is clear that after cycling in pristine electrolyte (6b insert) the space between the SiNWs is completely filled with the reduction products of electrolyte, which block the transport of lithium ions. Figure 6e insert shows that this space is free of reduction products. Since the diameter of native SiNWs is about 200 nm, the total thickness of the cycled SiNW is about 400 nm, the estimated SEI thickness is about 100 nm. This relatively thin SEI is usually detected when FEC is used.^[20]

3. Conclusions

A study of the solid electrolyte interphase (SEI) formation in a Si/Li battery containing a siloxane-based electrolyte has been carried out for the first time. On the basis of our electro-

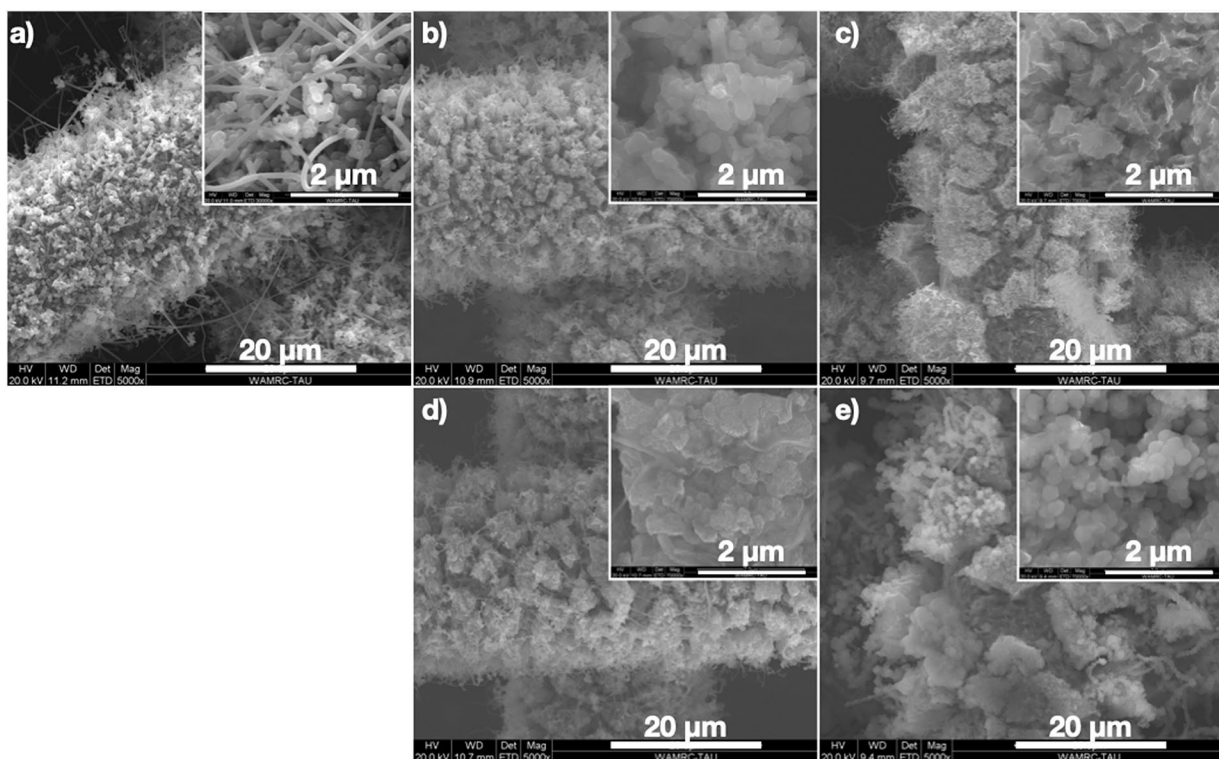


Figure 6. a) Ex-situ SEM images of Si nanowire anodes. b) The SiNW after 10 cycles at $25 \mu\text{A}$ between $1 \text{ V} \leqslant 0.05 \text{ V}$ in 1 mol kg^{-1} LiTFSI:TmdSx-CN and washed in water. c) Images of SiNWs after cycling under the same conditions stated above but with 10% (wt) FEC, and washed in water. d) The SiNWs from b), washed in DMC. e) The SiNWs from c) now washed in DMC. Main images were taken at $\times 5000$ magnification ($20 \mu\text{m}$), and the inset at $\times 70,000$ ($2 \mu\text{m}$) magnification.

chemical tests, it was deduced that TmdSx-CN forms a thick and dense SEI in contact with metallic lithium, as shown by in-situ electrochemical impedance spectroscopy (EIS), and polarization-modulation infrared-reflectance absorption spectroscopy (PM-IRRAS) spectra, and is supported by ex-situ scanning electron microscopy (SEM) images. Thus it enables only a few cycles before complete cell failure. Therefore, an additive, fluoroethylene carbonate (FEC) must be added to ensure good cycling satbility in TmdSx-CN electrolytes. Moreover, on the basis of X-ray photoelectron spectroscopy (XPS) depth profiles, we suggest that FEC is reduced more quickly than TmdSx-CN and TFSI and consequently mitigates the decomposition of the salt and the solvent by the reactions with lithium. We anticipate that “bi-functional end-group” solvents having a siloxane group at one end and a carbonate group at the other, will result in a single free-of-additives solvent that might produce an effective SEI.

Experimental Section

Chemicals

The 1,3-bis(cyanopropyl)tetramethyldisiloxane (TmdSx-CN, refer to Scheme 1) solvent was either purchased from ABCR (95%) or Sigma-Aldrich (97%), distilled under vacuum at least twice (106°C , 1×10^{-3} mbar) and dried for 24 hours over molecular sieves (3-4 Å) three times prior to use. Battery-grade fluoroethylene carbonate (FEC) was purchased from Solvay-Fluor. The lithium salt, lithium bis

(trifluoromethane)sulfonimide (LiTFSI) was purchased from 3M and dried at $100\text{--}120^\circ\text{C}$ under vacuum for at least 12 hours. The silicon nanowire (SiNW) anodes were synthesized in a catalyst-free CVD process described elsewhere.^[52] Metallic lithium was purchased from Rockwood Lithium Inc.

Coin Cells and Spectroelectrochemical Cell Assembly

The anodes were cut into 12 mm discs and dried under vacuum for 12 hours at 50°C , and 2 hours at 100°C . The mass loading of the anodes is $0.7\text{--}2.0 \text{ mg}_{\text{Si}} \text{ cm}^{-2}$, specific loading values are noted in the text. CR2032 coin cells were assembled inside an MBruan glovebox (O_2 and $\text{H}_2\text{O} < 0.1 \text{ ppm}$) filled with ultra-high-purified argon. The coin cells consisted of silicon composite anodes, a Celgard 2400 separator and a lithium foil counter electrode (Rockwood Lithium Inc). In spectroelectrochemical cells (EL-CELL) the cells functioned as three-electrode cells with a slab of metallic lithium as the reference electrode with a single glass-fibre separator (EL-CELL). The material for the optical window was CaF_2 . The standard electrolyte composition was 1 mol kg^{-1} LiTFSI in TmdSx-CN. For comparison, we added to the basic electrolyte, 10% (wt) of fluoroethylene carbonate (FEC). All cells were held at 30°C throughout the duration of the various experiments.

Electrochemical Stability

We tested the stability of SiNWs vs Li coin-cells by galvanostatic cycling, and probed the condition of the cell (SEI formation) by EIS. Typically, the procedure was as follows: 12 to 48 hours at rest, followed by an EIS measurement. Then, galvanostatic discharge at $I = -100 \mu\text{A}$ to 0.05 V vs LiLi^+ was carried out. Once the SiNWs were lithiated we carried out another EIS. To confirm the SEI

stability, the cell was equilibrated at open-circuit voltage (OCV) for three hours, followed by yet another EIS. After this, we charged (delithiated) at $I = +100 \mu\text{A}$ to 1.0 V vs Li^+/Li^- , discharged, and again charged the SiNWs to mimic the conditions under which one can reach a complete and steady SEI in carbonate-based materials on SiNWs.^[19,53] This was followed by two EIS measurements three hours apart at OCV. Finally, the cells were consecutively cycled at $\pm 100 \mu\text{A}$ between 1.0 V to 0.05 V for 25 cycles with an EIS measurement every five iterations.

PM-IRRAS Spectroscopy

We applied in-situ polarization modulation infrared reflectance absorption spectroscopy by a Nicolet iS50 equipped with a mercury-cadmium-telluride detector cooled by liquid nitrogen, and a PEM module instrument. Each PM-IRRAS spectrum was obtained by setting the modulation frequency (for maximum efficiency) at either 1500 cm^{-1} to probe the Si—O—Si spectral region or at 2900 cm^{-1} to probe the C—H spectral region. The resolution was set to 4 cm^{-1} . All profiles are the result of superimposing a total of at least 4000 interferograms. All spectra were processed with an Igor Pro 8 procedure for spline background correction.

FTIR Spectroscopy: FTIR spectra were measured with a Nicolet iS50 FT/IR Spectrometer (Thermo Fisher) with a diamond attenuated total reflectance (ATR) attachment.

Electrochemical Impedance Spectroscopy (EIS)

12 mm discs of the working electrodes, consisting of the stainless steel mesh coated with silicon nanowires were punched out, and dried in vacuum. These were assembled into a $\text{Li}|\text{separator}|\text{SiNW}$ configuration with a single 19 mm disc separator (Celgard 2400) in a 2032 coin cell. Coin cells were sealed in an MBraun glovebox with an argon environment, and removed from the glovebox for testing. We carried out EIS measurements with the use of a BioLogic VMP3 potentiostat with a frequency range of 1 MHz to 10 mHz. The initial impedance was measured after allowing the cell to equilibrate at open-circuit for 12 to 48 hours. The EIS results were analysed by the EC-lab software (Bio-logic). The bulk resistance (R_{bulk}) of the cell was determined by a circle fit to the resulting Nyquist plot and extracting the resistance associated with the high-frequency intercept.

X-Ray Photoelectron Spectroscopy (XPS)

XPS measurements were performed in UHV ($2.5 \times 10^{-10} \text{ Torr}$ base pressure) with the use of a 5600 Multi-Technique System (PHI, USA). The samples were irradiated by an Al K_α monochromatic source (1486.6 eV) and the resulting electrons were analysed by a Spherical Capacitor Analyzer with a slit aperture of 0.8 mm. The samples were charged during measurements, and this charging was compensated by means of a charge Neutralizer (C 1s at 285 eV was taken as an energy reference for all peaks). Samples were analysed at the surface and also after depth-profiling steps of 4 minutes with a 4 kV Ar^+ Ion Gun ($38.5 \text{ \AA min}^{-1}$ sputter rate on reference SiO_2/Si).

Scanning Electron Microscopy (SEM)

The morphology of soaked and cycled SiNWs anodes was measured with a FEI Quanta 200 FEG Environmental Scanning Electron Microscope (ESEM-EDS) system. Images were taken at $\times 270$ (500 μm), $\times 5000$ (20 μm), and $\times 70 \text{ k}$ (2 μm) magnifications with a beam energy of 20 kV.

Acknowledgements

This work was funded by the German/Israeli Battery School (GIBS) program, grant No. 00040024000. YH is supported by the Shamir Fellowship, graciously granted by Israel's Ministry of Science and Technology. YH wishes to express his gratitude for Dr. Kantor Uriel Nirit for fruitful discussions. We wish to thank Prof. Fernando Patolsky whose group provided us with the silicon nanowire samples.

Conflict of Interest

The authors declare no conflict of interest.

Keywords: batteries • disiloxanes • electrolytes • lithium • silicon

- [1] B. Scrosati, J. Garche, *J. Power Sources* **2010**, *195*, 2419.
- [2] T. Placke, R. Kloepsch, S. Dühnen, M. Winter, *J. Solid State Electrochem.* **2017**, *21*, 1939.
- [3] R. Schmuck, R. Wagner, G. Hörpel, T. Placke, M. Winter, *Nat. Energy* **2018**, *3*, 267.
- [4] G. Cauquis, D. Serve, *J. Electroanal. Chem. Interfacial Electrochem.* **1970**, *27*, A3.
- [5] J. Kasnatscheew, B. Streipert, S. Röser, R. Wagner, I. Cekic Laskovic, M. Winter, *Phys. Chem. Chem. Phys.* **2017**, *19*, 16078.
- [6] A. Vanchiappan, G. Joe, M. Srinivasan, L. Hua-Kun, *Chem. Eur. J.* **2011**, *17*, 14326.
- [7] L. J. Krause, W. Lamanna, J. Summerfield, M. Engle, G. Korba, R. Loch, R. Atanasoski, *J. Power Sources* **1997**, *68*, 320.
- [8] E. Kramer, S. Passerini, M. Winter, *ECS Electrochem. Lett.* **2012**, *1*, C9.
- [9] M. R. Wagner, P. R. Raimann, A. Trifonova, K.-C. Moeller, J. O. Besenhard, M. Winter, *Electrochem. Solid-State Lett.* **2004**, *7*, A201.
- [10] S. E. Renfrew, B. D. McCloskey, *J. Am. Chem. Soc.* **2017**, *139*, 17853.
- [11] J. Z. Olson, P. K. Johansson, D. G. Castner, C. W. Schlenker, *Chem. Mater.* **2018**, *30*, 1239.
- [12] S. Nowak, M. Winter, *J. Electrochem. Soc.* **2015**, *162*, A2500.
- [13] M. Winter, *Zeitschrift für Phys. Chemie* **2009**, *223*, 1395.
- [14] R. W. Schmitz, P. Murmann, R. Schmitz, R. Müller, L. Krämer, J. Kasnatscheew, P. Isken, P. Niehoff, S. Nowak, G.-V. Röschenthaler, N. Ignatiev, P. Sartori, S. Passerini, M. Kunze, A. Lex-Balducci, C. Schreiner, I. Cekic-Laskovic, *Prog. Solid State Chem.* **2014**, *42*, 65.
- [15] B. Pohl, M. M. Hiller, S. M. Seidel, M. Grünebaum, H.-D. Wiemhöfer, *J. Power Sources* **2015**, *274*, 629.
- [16] B. Pohl, M. Grünebaum, M. Drews, S. Passerini, M. Winter, H. D. Wiemhöfer, *Electrochim. Acta* **2015**, *180*, 795.
- [17] K. Amine, Q. Wang, D. R. Vissers, Z. Zhang, N. A. A. Rossi, R. West, *Electrochim. Commun.* **2006**, *8*, 429.
- [18] E. Markevich, G. Salitra, D. Aurbach, *ACS Energy Lett.* **2017**, *2*, 1337.
- [19] E. Peled, S. Menkin, *J. Electrochim. Soc.* **2017**, *164*, A1703.
- [20] I. A. Shkrob, J. F. Wishart, D. P. Abraham, *J. Phys. Chem. C* **2015**, *119*, 14954.
- [21] A. L. Michan, G. Divitini, A. J. Pell, M. Leskes, C. Ducati, C. P. Grey, *J. Am. Chem. Soc.* **2016**, DOI 10.1021/jacs.6b02882.
- [22] A. L. Michan, B. S. Parimalam, M. Leskes, R. N. Kerber, T. Yoon, C. P. Grey, B. L. Lucht, *Chem. Mater.* **2016**, DOI 10.1021/acs.chemmater.6b02282.
- [23] R. Ruffo, S. S. Hong, C. K. Chan, R. A. Huggins, Y. Cui, *J. Phys. Chem. C* **2009**, *113*, 11390.
- [24] J. P. Schmidt, T. Chrobak, M. Ender, J. Illig, D. Klotz, E. Ivers-Tiffée, *J. Power Sources* **2011**, *196*, 5342.
- [25] I. Rey, P. Johansson, J. Lindgren, J. C. Lassègues, J. Grondin, L. Servant, *J. Phys. Chem. A* **1998**, *102*, 3249.
- [26] G. Socrates, *Infrared and Raman Characteristic Group Frequencies: Tables and Charts*, John Wiley & Sons, **2001**.
- [27] R. Arnold, A. Terfort, C. Wöll, *Langmuir* **2001**, *17*, 4980.
- [28] R. J. Perry, M. J. O'Brien, *Energy Fuels* **2011**, *25*, 1906.
- [29] M. Hajzeri, L. S. Perše, M. Koželj, B. Orel, A. Šurca Vuk, *Sol. Energy Mater. Sol. Cells* **2015**, *139*, 51.

- [30] C. A. Hepburn, P. Vale, A. S. Brown, N. J. Simms, E. J. McAdam, *Talanta* **2015**, *141*, 128.
- [31] C.-W. Liew, H. M. Ng, A. Numan, S. Ramesh, *Polymer (Basel)* **2016**, *8*, 179.
- [32] J. F. Vélez, M. Aparicio, J. Mosa, *Electrochim. Acta* **2016**, *213*, 831.
- [33] J. Huang, A. F. Hollenkamp, *J. Phys. Chem. C* **2010**, *114*, 21840.
- [34] M. Kerner, N. Plylahan, J. Scheers, P. Johansson, *RSC Adv.* **2016**, *6*, 23327.
- [35] N. Mozhzhukhina, A. Y. Tesio, L. P. M. De Leo, E. J. Calvo, *J. Electrochem. Soc.* **2017**, *164*, A518.
- [36] F. Prieto, Z. Su, J. J. Leitch, M. Rueda, J. Lipkowski, *Langmuir* **2016**, *32*, 3827.
- [37] I. A. Profatilova, T. Langer, J. P. Badillo, A. Schmitz, H. Orthner, H. Wiggers, S. Passerini, M. Winter, *J. Electrochem. Soc.* **2012**, *159*, A657.
- [38] I. A. Profatilova, C. Stock, A. Schmitz, S. Passerini, M. Winter, *J. Power Sources* **2013**, *222*, 140.
- [39] R. E. Ruther, K. A. Hays, S. J. An, J. Li, D. L. Wood, J. Nanda, *ACS Appl. Mater. Interfaces* **2018**, *10*, 18641.
- [40] Y. Jin, N.-J. H. Kneusels, L. E. Marbella, E. Castillo-Martínez, P. C. M. M. Magusin, R. S. Weatherup, E. Jónsson, T. Liu, S. Paul, C. P. Grey, *J. Am. Chem. Soc.* **2018**, *140*, 9854.
- [41] D. J. Michalak, S. R. Amy, A. Esteve, Y. J. Chabal, *J. Phys. Chem. C* **2008**, *112*, 11907.
- [42] R. Younesi, P. Norby, T. Vegge, *ECS Electrochem. Lett.* **2014**, *3*, A15.
- [43] J. Barrio, A. Grafmüller, J. Tzadikov, M. Shalom, *Appl. Catal. B* **2018**, *237*, 681.
- [44] V. Etacheri, U. Geiger, Y. Gofer, G. A. Roberts, I. C. Stefan, R. Fasching, D. Aurbach, *Langmuir* **2012**, *28*, 6175.
- [45] C. C. Nguyen, B. L. Lucht, *J. Electrochem. Soc.* **2014**, *161*, A1933.
- [46] Z. L. Brown, S. Jurng, C. C. Nguyen, B. L. Lucht, *ACS Appl. Energy Mater.* **2018**, *1*, 3057.
- [47] P.-J. Alarco, Y. Abu-Lebdeh, A. Abouimrane, M. Armand, *Nat. Mater.* **2004**, *3*, 476.
- [48] G. G. Eshetu, T. Diemant, S. Grugeon, R. J. Behm, S. Laruelle, M. Armand, S. Passerini, *ACS Appl. Mater. Interfaces* **2016**, *8*, 16087.
- [49] Z. L. Brown, S. Jurng, C. C. Nguyen, B. L. Lucht, *ACS Appl. Energy Mater.* **2018**, DOI 10.1021/acsaem.8b00705.
- [50] A. Avila, I. Montero, L. Galán, J. M. Ripalda, R. Levy, *J. Appl. Phys.* **2000**, *89*, 212.
- [51] N. Li, P. Hu, X. Zhang, Y. Liu, W. Han, *Corros. Sci.* **2013**, *73*, 44.
- [52] N. Harpak, G. Davidi, D. Schneier, S. Menkin, E. Mados, D. Golodnitsky, E. Peled, F. Patolsky, *Nano Lett.* **2018**.
- [53] E. Peled, F. Patolsky, D. Golodnitsky, K. Freedman, G. Davidi, D. Schneier, *Nano Lett.* **2015**, *15*, 3907.

Manuscript received: November 15, 2018

Revised manuscript received: January 14, 2019

Accepted manuscript online: January 16, 2019

Version of record online: February 1, 2019